Journal of Photochemistry & Photobiology A: Chemistry 386 (2020) 112103

Contents lists available at ScienceDirect

Journal of Photochemistry & Photobiology A: Chemistry

journal homepage: www.elsevier.com/locate/jphotochem

Quinoline based probes: Large blue shifted fluorescent and electrochemical sensing of cerium ion and its biological applications

N. Bhuvanesh[a], S. Suresh[a], K. Velmurugan[a,b], A. Thamilselvan[c], R. Nandhakumar[a,*]

[a] Department of Chemistry, Karunya Institute of Technology and Sciences, (Deemed-to-be University), Karunya Nagar, Coimbatore, 641 114, India
[b] State Key Laboratory for Mechanical Behavior of Materials, Xi'an Jiaotong University, Xi'an, 710049, China
[c] Electro organic-devision, Central Electrochemical Research Institute (CSIR-CECRI), Karaikudi, 630 003, India

ARTICLE INFO

Keywords:
Fluorescence
ICT
Quinoline
Cerium ion
Electrochemical
Bio-imaging

ABSTRACT

Quinoline based fluorescent probes were formulated for the precise detection of cerium ions. Probes **1** and **2** detect Ce^{3+} ion as opposed to other metal ions through fluorescence in HEPES buffered CH_3CN-H_2O (1:1, (v/v) HEPES =50 mM, pH = 7.4) solution. The Ce^{3+} ion recognition process follows the π to π* transitions and intramolecular charge transfer (ICT) mechanisms. The LOD (Limit Of Detection) of probes **1** and **2** for sensing Ce^{3+} ion were found to be 1.60×10^{-9} M and 0.17×10^{-9} M, respectively. These probes are further utilized to detect Ce^{3+} ion by electrochemical studies. The practical applications of the probes are tested for varied biological applications.

1. Introduction

Cerium is a significant element in the lanthanum group and the most abundant of them. Also, most widely distributed among the "rare earths", averaging 22 mg kg^{-1} in the earth crust and found as ceric bastnaesite, monazite and silicate rocks [1]. Cerium is widely used in the production of ductile iron, cast iron, aluminum alloys and some stainless steels [2]. Cerium is indispensable for utility in industries such as metallurgy, glass and ceramics, lighting and television, and catalytic converters in vehicles [3]. However, cerium is hazardous in work environment as element fumes on inhalation can lead to lung embolisms, through prolonged exposure. Cerium is detrimental to liver tissue on accumulation in the body [4]. Due to its varied application in industry and society, there is growing interest in analyzing environmental, medical and biological effects of cerium. Therefore, the availability of precise methods for cerium determination is of importance. Ce^{3+} ion detection relies on varying instrumental methods, including spectrophotometry [5], X-ray fluorescence [6], inductively coupled plasma (ICP) [7–9], potentiometric sensors based on ion-selective electrodes [10–14], and spectrofluorometry [15–17]. Though these methods provide favorable results, the procedure involved is cumbersome. Several efforts have been undertaken to synthesize a precise sensor for Ce^{3+} ion [18–22]. Nevertheless, they suffer from narrow working pH range [20,21], concentration range [19,21], and longer response time [19]. In this regard, ongoing fluorescent studies are targeted towards the development of a precise sensor system for selective detection of cerium ions with high sensitivity [23–25]. A fluoroionophore system showing high selectivity for Ce^{3+} ion in semi-aqueous solution associated with fluorescent changes are important implications can be used as specific chemosensors. As well as, reports on electrochemical detection of Ce^{3+} ion is apparently rare. Reports are obtainable for Ce^{3+} ion determination constructed on adsorptive stripping voltammetry and cyclic voltammetry techniques [26]. Electrochemical sensors for Ce^{3+} ion estimation in drinking water and sea water are reported [27]. Here, we report that the two symmetrical dimeric quinolone isomers **1** and **2** are used as fluorescent as well as electrochemical sensors for Ce^{3+} ion, which is free from the interferences of other metal ions. Therefore, to the better of our understanding this is the first report on two symmetrical dimeric quinoline isomers **1** and **2**, which are modulated by the linkers showed almost the same selectivity towards Ce^{3+} ion with a large blue shift irrespective of their position monitored by fluorescence studies. These electrochemical fluorescent probes **1** and **2** exhibit affinity for the sensing of Ce^{3+} ion observed through distinct fluorescence changes denoted by blue shift responses due to Intramolecular Charge Transfer (ICT) process in CH_3CN–H_2O (1:1 v/v, HEPES =50 mM, pH = 7.4) solutions.

* Corresponding author.
E-mail address: nandhakumar@karunya.edu (R. Nandhakumar).

https://doi.org/10.1016/j.jphotochem.2019.112103
Received 2 May 2019; Received in revised form 17 August 2019; Accepted 21 September 2019
Available online 23 September 2019
1010-6030/

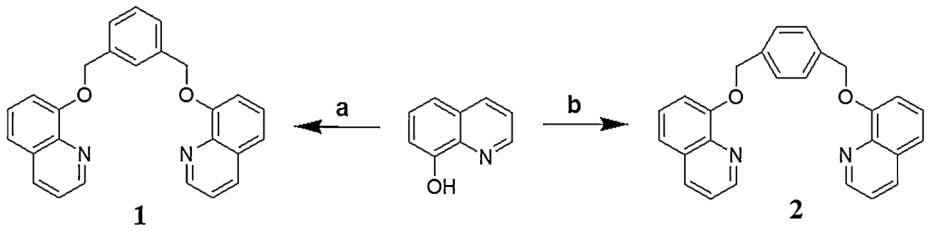

(a) α,α′-dibromo-m-xylene, CH_3CN, K_2CO_3, reflux, 16 h. (b) α,α′-dibromo-p-xylene, CH_3CN, K_2CO_3, reflux, 16 h.

Scheme 1. Synthesis of probes **1** and **2.**
(a) α,α′-dibromo-m-xylene, CH_3CN, K_2CO_3, reflux, 16 h. (b) α,α′-dibromo-p-xylene, CH_3CN, K_2CO_3, reflux, 16 h.

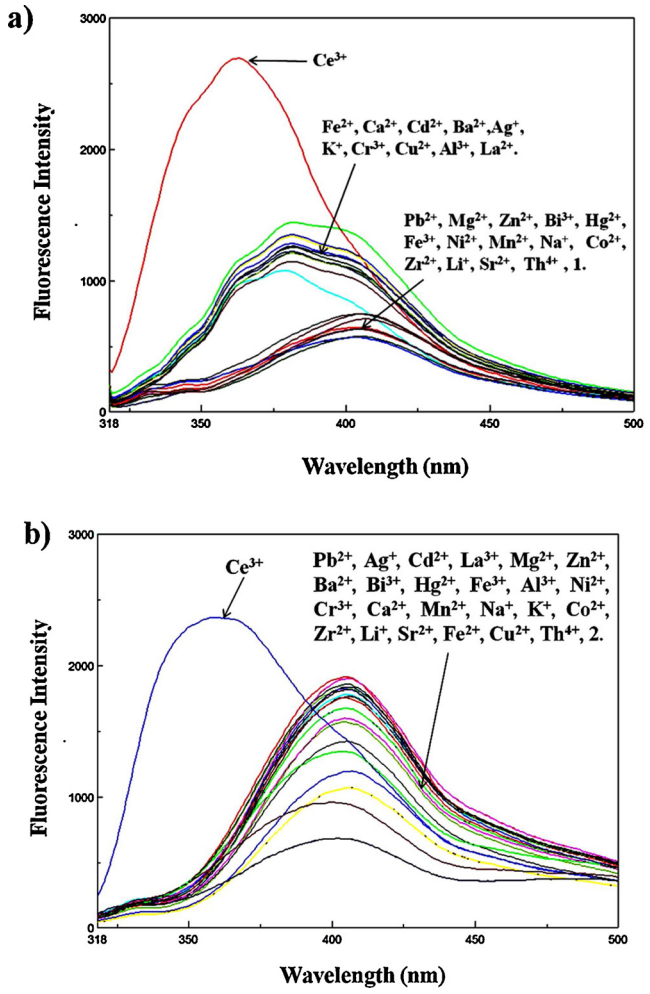

Fig. 1. Fluorescence spectral changes of the probes a) **1** and b) **2** (4 μM) with significant metal ions (100 equiv.) were added in CH_3CN-H_2O (1:1 (v/v), HEPES =50 mM, pH = 7.4) solution. (λ_{ex} = 308 nm).

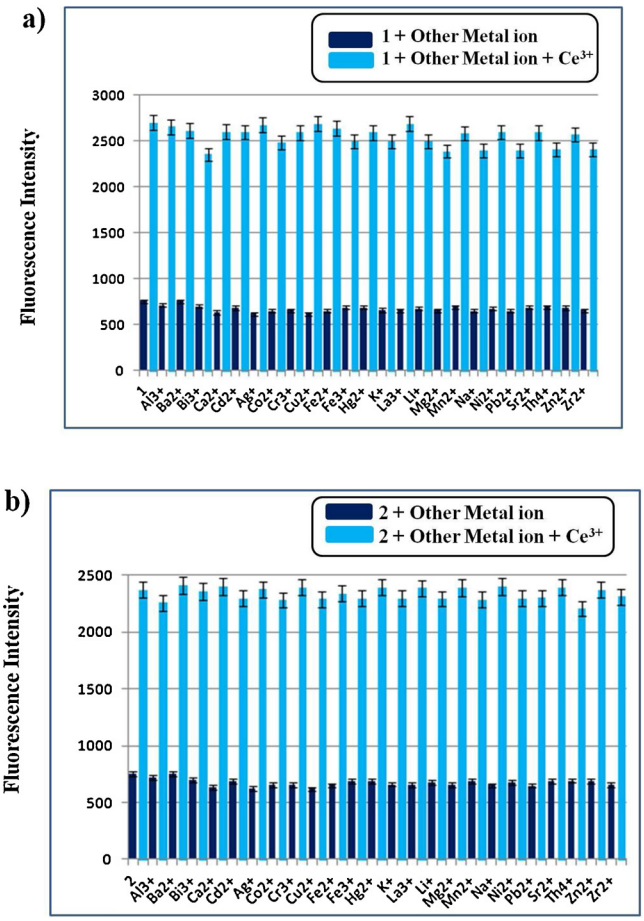

Fig. 2. Competition analysis of the probes a) **1** and b) **2** in CH_3CN-H_2O (1:1 (v/v), HEPES =50 mM, pH = 7.4) solution. The purple bars denote fluorescence emission of probes **1** and **2** and 100 equiv. of other metal ions. The sky blue bars denote variation fluorescence that occur upon addition of 100 equiv. of other significant metal ions to the solution containing probes **1** and **2** and Ce^{3+} ion (100 equiv.). The error bars represent the standard deviation of three measurements.

2. Experimental section

2.1. Materials and instruments

All procured solvents are HPLC grade quality. α,α′-Dibromo-*m*-xylene, α,α′-Dibromo-*p*-xylene and 8-Hydroxyquinoline and were sourced from Sigma Aldrich. Boetius Microheating Table and Mettler-FP5 Melting apparatus were used to measure the melting points. ^1H and ^{13}C NMR spectra were noted on a Bruker 400 and 100 MHz spectrometer, respectively, in $CDCl_3$ solution with TMS as an internal standard. LC–MS was determined by utilizing infusion methods. Absorption spectra was examined using a Jasco UV-630 spectrophotometer. Fluorescence measurement was recorded utilizing a Jasco FP-8200 spectrofluorometer equipped with quartz cuvettes of 1 cm path length. The excitation and emission slit widths were 2.5 nm. All absorption and emission spectra were recorded at 24 ± 1 ^{0}C. Stock solutions for analysis were prepared (2×10^{-3} M for probes **1** and **2** (CH_3CN/H_2O, 1:1 (v/v), HEPES =50 mM, pH = 7.4) immediately before the experiments. The solutions of metal ions were prepared from the nitrate salts

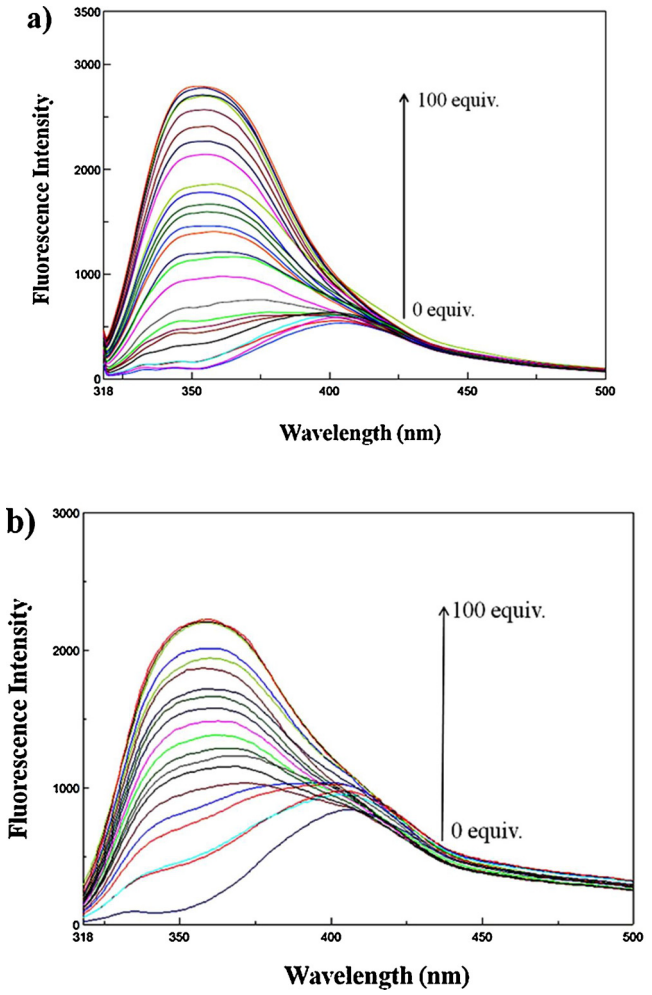

Fig. 3. Variance in fluorescence intensity of the probes a) **1** and b) **2** (4 μM) on rising concentration of Ce^{3+} ion (0–100 equiv.) in CH_3CN-H_2O (1:1 (v/v), HEPES = 50 mM, pH = 7.4) solution. (λ_{ex} = 308 nm).

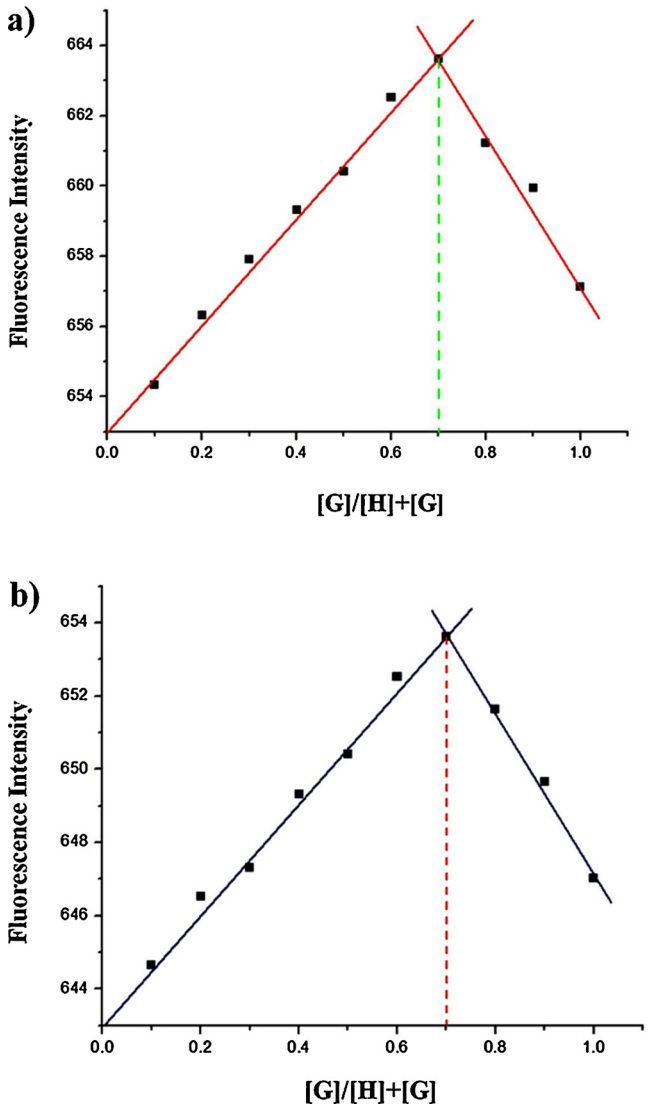

Fig. 4. Job's plot of the probes a) **1** and b) **2** with Ce^{3+} ion in CH_3CN-H_2O (1:1 (v/v), HEPES = 50 mM, pH = 7.4) solution. (λ_{ex} = 308 nm).

of Pb^{2+}, Cu^{2+}, Cd^{2+}, Hg^{2+}, La^{3+}, Zn^{2+}, Co^{2+}, Ni^{2+}, Ca^{2+}, Mn^{2+}, Cr^{3+}, Ba^{2+}, Bi^{3+}, Ce^{3+}, Mg^{2+}, Al^{3+}, Fe^{2+}, Fe^{3+}, Ag^{+}, Zr^{2+}, Th^{4+}, Li^{+}, Sr^{2+}, Na^{+} and K^{+}.

2.2. Synthesis

2.2.1. 8-(3-((quinolin-8-yloxy)methyl)benzyloxy)quinoline (1)

Probe **1** was prepared by dissolving α,α′-dibromo-*m*-xylene (0.50 g, 1.90 mmol) and 8-hydroxyquinoline (0.60 g, 4.18 mmol) in acetonitrile (50 mL) in the presence of potassium carbonate and refluxed for 16 h. After the reaction completed, monitored by TLC, the formed precipitate was filtered and washed with more ice cold acetonitrile. The crude product was further purified by column chromatography afforded as **1**. Yield = 85%. m.p. 273–276 ^{0}C. ^{1}H NMR (400 MHz, $CDCl_3$) δ: 8.83–8.85 (d, J = 6 Hz, 2 H), 7.97–8.00 (d, J = 9 Hz, 2 H), 7.56 (s, 1 H), 7.06–7.38 (m, 9 H), 6.87–6.90 (m, 2 H), 5.31 (s, 4 H) ppm. ^{13}C NMR (100 MHz, $CDCl_3$): δ 153.86, 148.73, 139.88, 137.16, 136.21, 129.43, 128.87, 126.69, 125.92, 121.57, 119.76, 109.90, 77.33, 57.69 ppm. Elemental analysis: $C_{26}H_{20}N_2O_2$: Calc.; C, 80.75; H, 4.84; N, 6.73%, Found; C, 80.70; H, 4.75; N, 6.68%. LC–MS Calcd. for $C_{26}H_{20}N_2O_2$: $[M^+]$ 392, found $[M+H]^+$ 393.

2.2.2. 8-(4-((quinolin-8-yloxy)methyl)benzyloxy)quinoline (2)

Probe **2** was prepared similar to probe **1**, except α,α′-dibromo-*p*-xylene is used instead of α,α′-dibromo-*m*-xylene. Yield = 82%. m.p. 275–279 ^{0}C. ^{1}H NMR (300 MHz, $CDCl_3$) δ: 8.95–8.96 (d, J = 3 Hz, 2 H), 8.09–8.12 (d, J = 9 Hz, 2 H), 7.33–7.51 (m, 10 H), 7.00–7.03 (m, 2 H), 5.42 (s, 4 H) ppm. ^{13}C NMR (101 MHz, $CDCl_3$) δ: 154.26, 149.37, 140.44, 136.61, 135.95, 129.51, 127.49, 126.61, 121.62, 119.90, 109.92, 77.08, 70.51 ppm. Elemental analysis: $C_{26}H_{20}N_2O_2$: Calc.; C, 79.57; H, 5.14; N, 7.14%, Found; C, 79.53; H, 5.12; N, 7.11%. LC–MS Calcd. for $C_{26}H_{20}N_2O_2$: $[M^+]$ 392, found $[M+H]^+$ 393.

2.2.3. Electrochemical studies

The electrochemical properties of the probes were evaluated using cyclic voltammetry (CV) with CH_3CN as a solvent (BioLogic SP-150 Potentiostats, France), Tetrabutyl ammonium perchlorate (TBAP), Glassy carbon (GC) working electrode, convectional three-electrode cell at room temperature. For the electrochemical studies, GC and Pt were used as working and reference electrodes respectively, where Ag/AgCl served as reference electrode. The supporting electrolyte TBAP was melted and dried under vacuum for one hour. Probes **1** and **2** were measured at 2×10^{-5} M concentration with 0.1 M of supporting electrolyte. These solutions were degassed by bubbling nitrogen before experiments. The cyclic voltammetry was performed in the potential range of +0.5 to -2.5 V (*vs* SCE) in which the applied potential was ramped between -2.5 V and +0.5 V (*vs* SCE) for oxidation of quinoline molecules and subsequently, the applied potential was ramped between

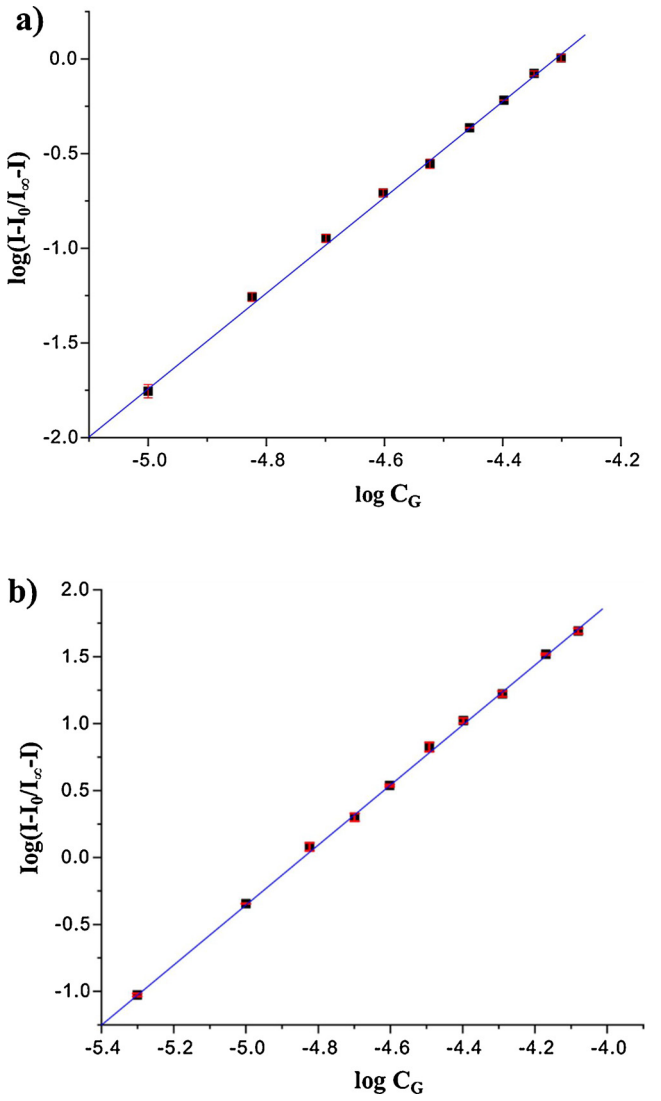

Fig. 5. Benesi–Hildebrand plot of the probes a) **1**:Ce^{3+} (1:2) and b) **2**:Ce^{3+} (1:2) complexes binding stoichiometry ($\lambda_{ex.}$ = 308 nm). Error bars represent standard deviations from three-times repeated experiments.

+0.5 V and -2.5 V (*vs* SCE) for the reduction of quinoline molecules.

2.2.4. Antibacterial and antifungal activity

Assay of antibacterial activity by means of disc diffusion method using nutrient agar medium against two pathogenic bacteria *Staphylococcus aureus* and *Escherichia coli* were performed. Kanamycin and Chloramphenicol were used as controls in a sterile disc of whatman No.3 grade. An equal amount of the samples added on the discs with at most care and placed on an agar surface and incubated at 37 °C for 24 h. Inhibition zone was measured and recorded. Similarly, the assay of antifungal activity was performed by means of well diffusion method against *Aspergillus flavus* on the potato dextrose agar (PDA) medium. The samples were added on the well against the pathogenic fungi and incubated at 25 °C for 2 days. After a sufficient incubation period, the inhibition zone was measured and recorded.

3. Results and discussion

3.1. Synthesis of probes 1 and 2

The dimeric quinoline based probes **1** and **2** were prepared by utilizing condensation reaction involving two positional isomers of dibromoxylene and 8-hydroxyquinoline in acetonitrile solution at reflux condition for 16 h (Scheme 1). The molecular symmetry of the probes was analyzed utilizing NMR and Mass Spectroscopy (Fig. S1-S3).

3.2. Evaluation of selectivity

Fluorescence spectroscopic technique was used to evaluate the selectivity and sensitivity of probes **1** and **2** with respect to specific ions of environmental significance, such as Pb^{2+}, Cu^{2+}, Cd^{2+}, Hg^{2+}, La^{3+}, Zn^{2+}, Co^{2+}, Ni^{2+}, Ca^{2+}, Mn^{2+}, Cr^{3+}, Ba^{2+}, Bi^{3+}, Ce^{3+}, Mg^{2+}, Al^{3+}, Fe^{2+}, Fe^{3+}, Ag^{+}, Zr^{2+}, Th^{4+}, Li^{+}, Sr^{2+}, Na^{+} and K^{+}. Before starting the fluorescence measurements, the UV–vis absorption spectra of probes **1** and **2** in CH_3CN-H_2O (1:1 (v/v), HEPES = 50 mM, pH = 7.4) at different concentrations were measured and the excitation wavelength was fixed at λ_{ex} = 308 nm (Fig. S4). The metal ion sensing analysis was carried out by adding a specified concentration of various metal salts in CH_3CN-H_2O (1:1 (v/v), HEPES = 50 mM, pH = 7.4) to a fixed concentration of probes **1** and **2** in the same solvents. In a typical experiment, addition of Ce^{3+} ion to the probes **1** and **2** induces a dramatic enhancement in the fluorescence spectra upon excitation at 308 nm. It is worthwhile to note that, there is a significant hypsochromic shift from 405 nm to 360 nm during the course of the fluorescence enhancement, which reveals that there is an ICT process involved after the cerium ion coordination with the probes **1** and **2** (Fig. 1). As a result, probes **1** and **2** exhibit a selective Ce^{3+} ion affinity as compare to potentially significant metal ions through fluorescence responses with a possible ICT mechanism even though being symmetrical, the probes differ in the position of their linker.

3.3. Effect of pH and time response

Fluorescence responses of probes **1** and **2** with Ce^{3+} ions at varying pH range are vital to assess the photophysical properties of probes **1** and **2**. The sensitive detection of Ce^{3+} ion using probes **1** and **2**, over a different pH range in CH_3CN/H_2O (1:1 (v/v)) solution was therefore performed. The results indicate that there is no change in the fluorescence intensity among probes **1** and **2** over a wide pH range. However, peak emissions in **1** + Ce^{3+} and **2** + Ce^{3+} were observed between 7–9 and 6–8 pH ranges, respectively (Fig. S5). These results demonstrated that probes **1** and **2** bind with Ce^{3+} ion over the pH range with increased fluorescence intensity. Therefore, based on the above, an optimal pH of 7.4 is applied throughout the experiments for both the probes **1** and **2**. At the same time, changes in fluorescence intensities of probes **1** and **2** against time were also performed (Fig. S6). The fluorescence intensities of probes **1** and **2** peaked within 2 and 3 min, respectively. The peak intensities were stabilized for further 50 min upon the addition of Ce^{3+} ions to probes **1** and **2.** These results highlight the fact that probes **1** and **2** favorably detects Ce^{3+} ion within a short span of time hold promising applications in environmental and biological media.

3.4. Binding stoichiometric studies

The precision sensing behavior of probes **1** and **2** for detecting Ce^{3+} ion was analyzed by utilizing other metal ions of biological and environmental significance (Fig. 2). To check the efficacy of probes **1** and **2** for the detection of Ce^{3+} ion (100 equiv.), similar concentration of (100 equiv.) competing the metal ions namely Pb^{2+}, Cu^{2+}, Cd^{2+}, Hg^{2+}, La^{3+}, Zn^{2+}, Co^{2+}, Ni^{2+}, Ca^{2+}, Mn^{2+}, Cr^{3+}, Ba^{2+}, Bi^{3+}, Mg^{2+}, Al^{3+}, Fe^{2+}, Fe^{3+}, Ag^{+}, Zr^{2+}, Th^{4+}, Li^{+}, Sr^{2+}, Na^{+} and K^{+} were added to those probes. These results indicated that no significant variance in a precision detection property of the probes in the presence of competing metal ions.

The variance in fluorescence intensity of probes **1** and **2** was monitored by on steadily raising the concentration of Ce^{3+} ions as shown in Fig. 3. Upon increasing the concentrations of Ce^{3+} ion to probes **1** and

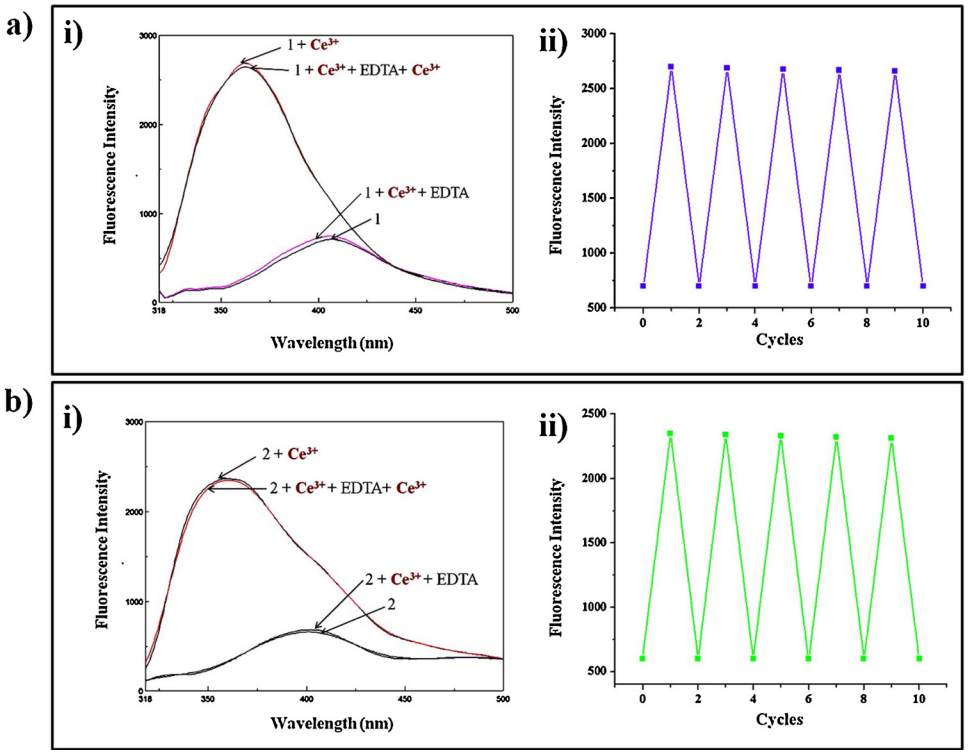

Fig. 6. Variance in fluorescence spectra of a) (i) probe **1** and b) (i) probe **2** (4×10^{-6} M) in CH_3CN-H_2O (1:1 (v/v), (HEPES = 50 mM, pH = 7.4) in the presence of Ce^{3+} ion and EDTA (100 equiv.). a) (ii) and b) (ii) in number of cycles used for the recognition of Probes **1** and **2**/Ce^{3+}.

2, the fluorescence intensity gradually increased with an interesting and prominent blue shift from 405 to 360 nm. The fluorescence intensity peaked after the addition of 100 equiv. of Ce^{3+} ion. Importantly, the titration profile reveals that the probes **1** and **2** interact with Ce^{3+} ion in 1:2 binding stoichiometry, respectively. As a result, maximum mole fraction was observed at 0.7 and 0.7, which indicates 1:2 and 1:2 (H:G) binding stoichiometry between probes **1** and **2** with Ce^{3+} complex (Fig. 4). The **1**-Ce^{3+} (1:2) and **2**-Ce^{3+} (1:2) complexes binding stoichiometry were further corroborated by the LC-Mass spectral analysis, there is a peak at *m/z* 1043 shown in supporting information as direct evidence of the complex formation (Fig. S7). Moreover, the molecular ion peak at *m/z* 1043, which corresponds to the [**1** + $(Ce(NO_3)_3]$ complex were depicted in the mass spectrum. Based on fluorescence titration profiles, the binding stoichiometric ratio of **1**-Ce^{3+} (1:2) and **2**-Ce^{3+} (1:2) complexes were analyzed utilizing the Benesi–Hildebrand equations (Fig. 5) [28–32]. Therefore, probes **1** and **2** possess the binding constant values as $K_a = 9.23 \times 10^7$ M^{-2} and $K_a = 9.44 \times 10^7$ M^{-2}, respectively. The limit of detection (LOD) ranges [33–35] of Ce^{3+} ion marginally varied for probes **1** and **2**, which were determined as 1.60×10^{-9} M and 0.17×10^{-9} M, respectively. These values were determined using the equation $3\delta/S$, where δ denotes the standard deviation of the free probe, and S denotes the slope of the linear regression plot obtained in the titration spectral data.

3.5. Reversibility of probes 1 and 2

The recycling ability of probes **1** and **2** to the detection of Ce^{3+} ion is critical requirements. This study examined the reversibility of binding between **1**-Ce^{3+} and **2**-Ce^{3+} in the presence of EDTA (100 equiv.) in CH_3CN-H_2O (1:1 (v/v), HEPES = 50 mM, pH = 7.4) solution. The combining of EDTA (100 equiv.) to the solutions containing probes **1** and **2** with Ce^{3+} ion resulted in the elimination of fluorescence signals of **1**-Ce^{3+} and **2**-Ce^{3+}, and attainment of original intensity of free probes **1** and **2**. These results indicate the reversibility in Chelation process as depicted in Fig. 6a (i) and 6b (i) for probes **1** and **2**. This reversibility of probes **1** and **2** was verified through repeated experiments and results indicated that probes can be utilized in more than 10 instances for the detection of Ce^{3+} ion (Fig. 6a (ii) and 6b (ii)).

3.6. Proposed binding mode of the complex

The binding mechanism of the probes was examined by utilizing the variations observed in fluorescence, as depicted in Scheme 2. Probes **1** and **2** exhibited a weak fluorescence, which is due to n to π* transitions appeared by hetero atoms. Upon addition of Ce^{3+} ions to probes **1** and **2**, the fluorescence enhancement was observed with considerable blue shift, which is due to an internal Intramolecular Charge Transfer (ICT) process between two quinoline rings. Possibly, the two hetero atoms 'N' and 'O' of the two quinoline rings are engaged on the complexation with Ce^{3+}, which leads to the hindrance of n to π* transitions and π to π* transitions are allowed. Hence, the dangling quinoline rings attached to the xylylene ring through a freely rotatable oxygen atom, eventually become rigid. Therefore, the feasible coordination modes of **1**-Ce^{3+} and **2**-Ce^{3+} complexes based on the data obtained from Job's plot, non-linear curve fitting (Benesi-Hildebrand) methods and mass spectra results in a 1:2 (Host: Guest) binding stoichiometry.

3.7. IR spectral analysis

The IR spectral analysis of probe **1** and **1**-Ce^{3+} complex were recorded. As depicted in (Fig. S8a), the IR spectra of probe **1** displayed specific bands that appeared at 1382 cm^{-1} and 1632 cm^{-1} relating to C—O and C═N groups on the quinoline moiety, respectively [36]. Upon addition of Ce^{3+} ion to probe **1**, there is a significant shift in its absorption bands from 1382 cm^{-1} and 1632 cm^{-1} to 1373 cm^{-1} and 1627 cm^{-1}, due to slump in the electron density of the quinoline rings. These band shifts can be attributed to the alignment of Ce^{3+} ion with the C—O and C═N groups of probe **1**. Similarly, the IR spectral analysis of probe **2** displayed specific absorption bands at 1374 cm^{-1} and 1625 cm^{-1} relating to C—O and C═N groups on the quinoline moiety,

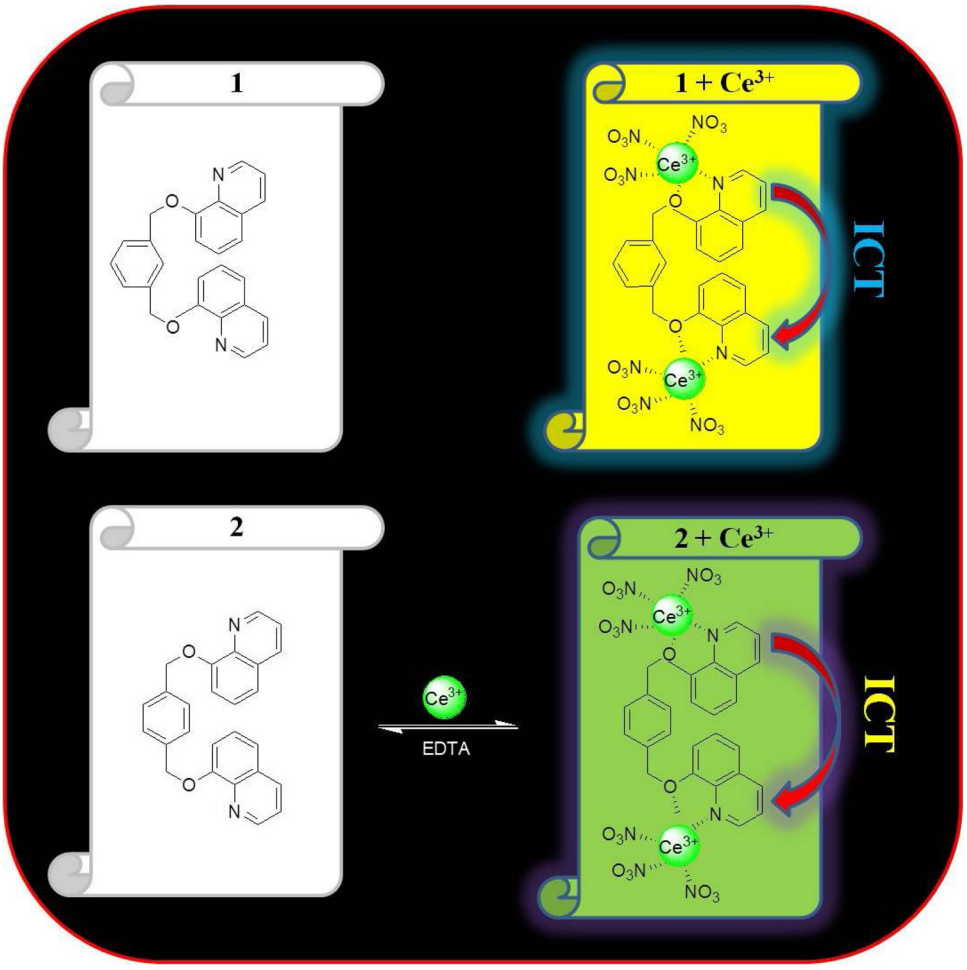

Scheme 2. Possible binding mode of the probes **1** and **2** with $Ce(NO_3)_3$.

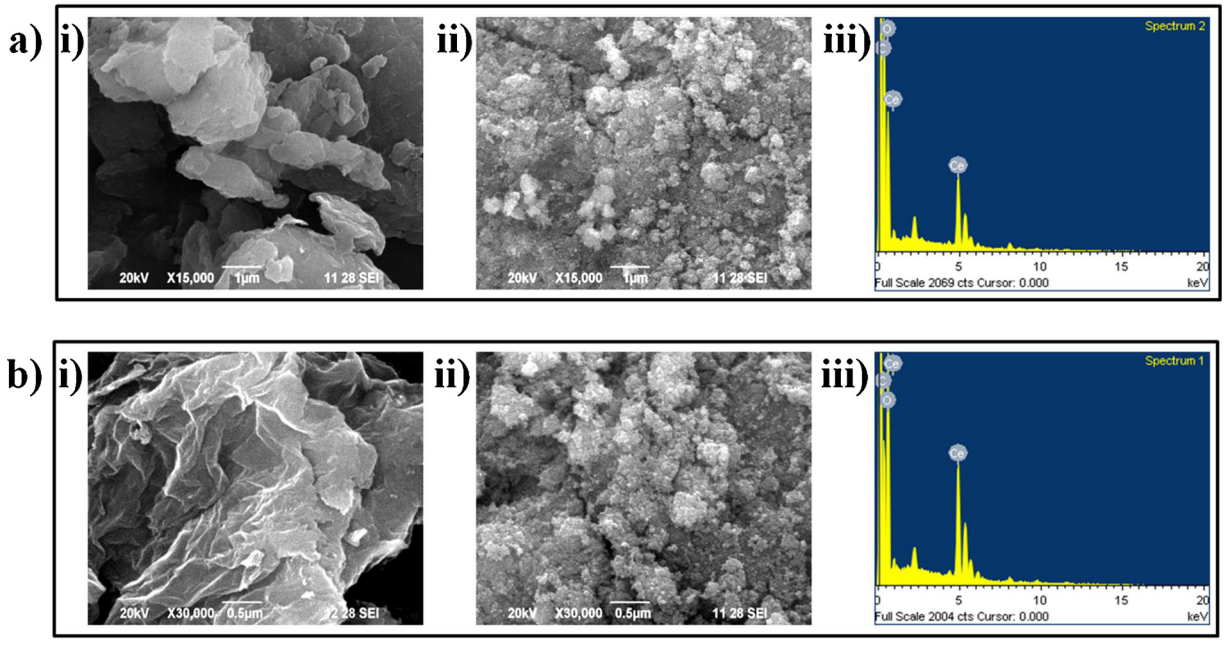

Fig. 7. Scanning Electron Micrograph of a) i) Probe **1** only ii) **1** + Ce^{3+} and b) i) Probe **2** only ii) **2** + Ce^{3+} and EDAX analysis of a) iii) **1** + Ce^{3+} and b) iii) **2** + Ce^{3+} complex.

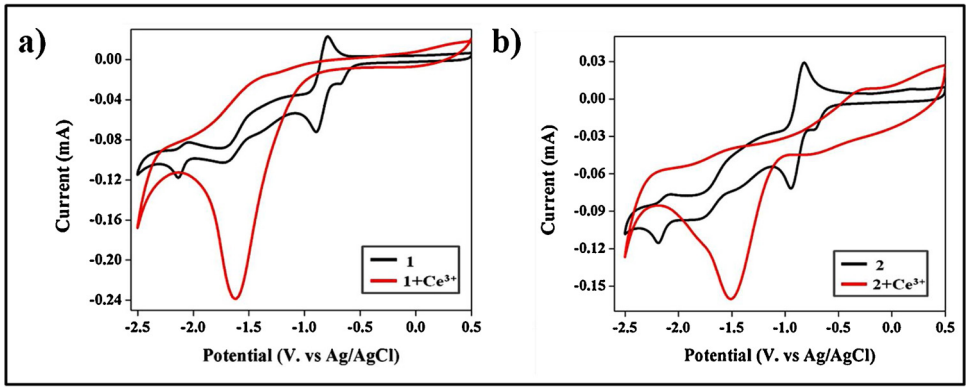

Fig. 8. Cyclic voltammogram obtained on a) and b) both probes **1** and **2** (2×10^{-5} M) with $Ce(NO_3)_3$ (100 equiv) 0.1 M of TBAP supporting electrolyte in acetonitrile.

Table 1
A comparison between Fluorescence and Electrochemical detection mode.

Sample	Limit Of Detection (LOD)	
	Fluorescence Detection	Electrochemical Detection
1 with Ce^{3+}	1.60×10^{-9} M	1.65×10^{-9} M
2 with Ce^{3+}	0.17×10^{-9} M	0.19×10^{-9} M

respectively (Fig. S8b). Upon addition of Ce^{3+} ion to probe **2**, there is a significant shift in its absorption bands from 1374 cm^{-1} and 1625 cm^{-1} to 1370 cm^{-1} and 1623 cm^{-1}, respectively. These band shifts are possibly due to the coordination of Ce^{3+} ion with the C—O and C═N groups of probe **2**.

3.8. Microscopic studies

The SEM images of probes **1, 2, 1** + Ce^{3+} and **2** + Ce^{3+} revealed that some noticeable changes in surface topography as displayed in Fig. 7. SEM images of probes **1** and **2** possess a stone-like structure and morphed to spherical-like structure on interaction with **Ce^{3+}** ion. This can be attributed to the agglomeration of probes **1** and **2** with Ce^{3+} ion. The chemical composition of the probes **1** + Ce^{3+} and **2** + Ce^{3+} complexes were measured by EDAX analysis (Fig. 7a (iii) and 7b (iii)) indicates the presence of carbon (C), oxygen (O) and Cerium (Ce) elements in the probes **1** + Ce^{3+} and **2** + Ce^{3+} complexes, respectively.

Table 2
Selected electrochemical properties of probes **1** and **2** upon addition of different metal ions.

S. No	Probe	E_{pa} (V)
1	**1**	−0.89
2	**1 with Ce^{3+}**	**−1.62**
3	**1** with Al^{3+}	−0.98
4	**1** with Fe^{2+}	−0.93
5	**1** with Ni^{2+}	−0.81
6	**2**	−0.94
7	**2 with Ce^{3+}**	**−1.51**
8	**2** with Al^{3+}	−0.95
9	**2** with Fe^{2+}	−0.91
10	**2** with Ni^{2+}	−0.88

3.9. Application studies

3.9.1. Electrochemical behavior of probes 1 and 2 with Ce^{3+} ions

The electrochemical properties of probes **1** and **2** were examined in CH_3CN. For contrast purposes, the solutions were shielded, as were their protonated derivatives that are vulnerable to light. A typical cyclic voltammogram (CV) of probe **1** is depicted in Fig. 8. This validates similarity in that the electrochemical characteristics of probes **1** and **2.** Consequently, the CV of free probes **1** and **2** and probes **1** and **2** containing 100 equiv. of respective metal ions Ce^{3+}, Al^{3+}, Fe^{2+} and Ni^{2+} were measured. This electrochemical trend depicted in Fig. 8 been observed for respective probes, where quinoline groups realigned with regard to meta and para position. In oxidation, the initial peak corresponds to a reversible and elaborate oxidation process of probes **1** and **2**. This peak can be an outcome of oxidation of the quinoline moiety [37–40] whose first oxidation potential is -0.89 and -0.94 V in probes **1**

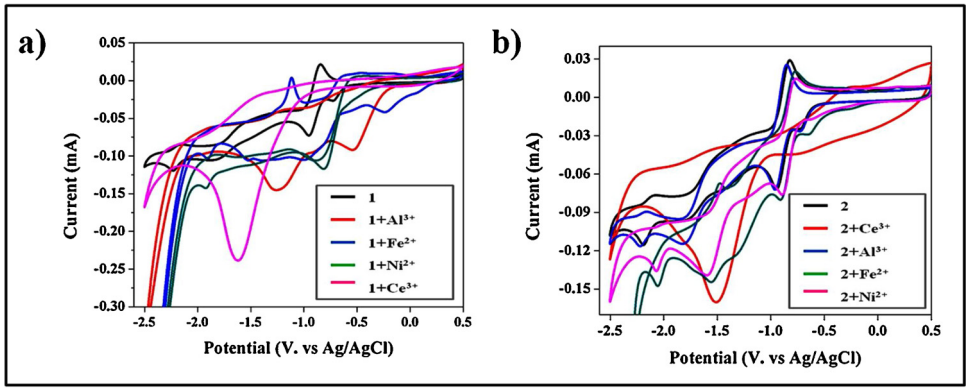

Fig. 9. Cyclic voltammogram of a) and b) both probes **1** and **2** with other metal ions of Al^{3+}, Fe^{2+}, Ni^{2+} (100 equiv) 0.1 M of TBAP supporting electrolyte in acetonitrile.

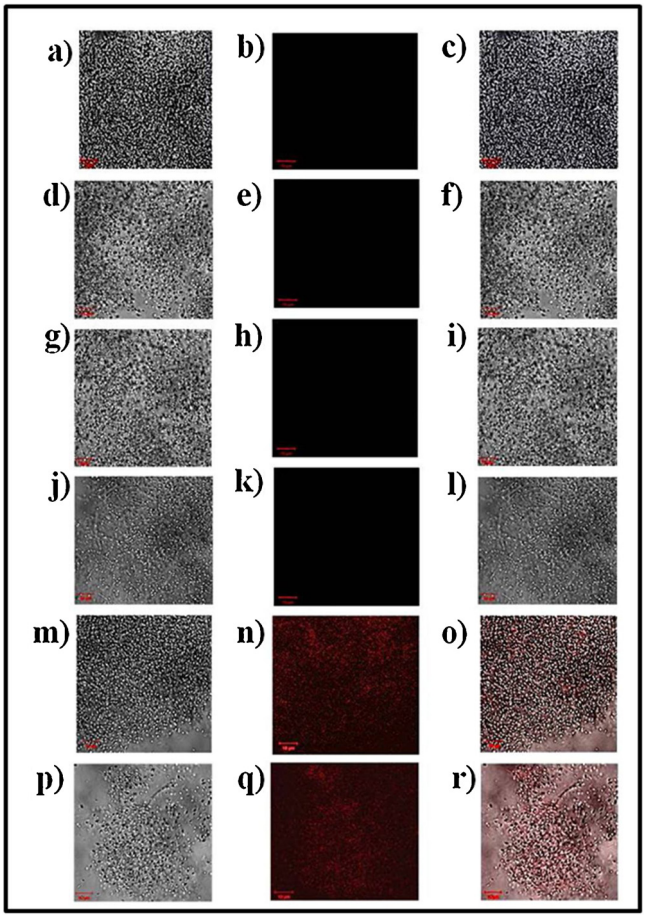

Fig. 10. Laser confocal scanning microscopic images of (a) Bright field image of *E. coli* cells, (b) Confocal image of *E. coli* cells, (c) Super imposed image of (a) and (b), (d) Bright field image of *E. coli* cells stained using probe **1** (10 μM), (e) Confocal image of *E. coli* cells stained to only probe **1** (10 μM), (f) Super imposed image of (d) and (e), (g) Bright field image of *E. coli* cells stained using probe **2** (10 μM), (h) Confocal image of *E. coli* cells stained to only probe **2** (10 μM), (i) Super imposed image of (g) and (h), (*j*) Bright field image of *E. coli* cells stained using Ce^{3+} ion (20 μM), (k) Confocal image of *E. coli* cells stained to Ce^{3+} ion (20 μM), (l) Super imposed image of (*j*) and (k), (m) Bright field image of *E. coli* cells stained to probe **1** (10 μM) and Ce^{3+} ion (20 μM), (n) Confocal image of E. coli cells stained using probe **1** (10 μM) and Ce^{3+} ion (20 μM), (o) Super imposed image of (m) and (n), (p) Bright field image of *E. coli* cells stained to probe **2** (10 μM) and Ce^{3+} ion (20 μM), (q) Confocal image of E. coli cells stained using probe **2** (10 μM) and Ce^{3+} ion (20 μM), (r) Super imposed image of (p) and (q), in CH_3CN-HEPES (1:1, v/v) solution.

Table 3
Antimicrobial activity of probes **1** and **2** with Ce^{3+} ions against *Staphylococcus aureus, Escherichia coli and Aspergillus flavus.*

Sample	Zone of Inhibition (mm)		
	Staphylococcus aureus	*Escherichia coli*	*Aspergillus flavus*
Control	27 mm	25 mm	–
1	–	–	2 mm
2	10 mm	–	10 mm
1 with Ce^{3+}	26 mm	22 mm	15 mm
2 with Ce^{3+}	13 mm	4 mm	20 mm

- No growth beneath the disc.

and **2**. Interestingly, on addition of Ce^{3+} ion, the detection properties of probes **1** and **2** were different and the LOD (Limit Of Detection) of probes **1** and **2** for sensing Ce^{3+} ion were found to be 1.65×10^{-9} M and 0.19×10^{-9} M, respectively (Table 1). The anodic shift of oxidation potential of probe **1** moved from -0.89 V to -1.62 V and probe **2** moved from -0.94 V to -1.51 V, respectively. The above CV experiments also performed to prove the probes **1** and **2** selectively towards Ce^{3+} ions (Fig. 8). Under similar circumstances, probes **1** and **2** on addition of specific metal ions such as Al^{3+}, Fe^{2+}, and Ni^{2+} displayed no significant variation in oxidation potential as depicted in Fig. 9. This dip in oxidation potential can be a result of ICT between dimeric quinoline probes. All the above results revealed that the probes **1** and **2** have greater affinity for Ce^{3+} ion in contrast to other metal ions. Considering these findings, the order of selectivity can be seen. *i.e.* $Ce^{3+} > Al^{3+} > Fe^{2+} > Ni^{2+}$ (Table 2).

3.9.2. Biological applications

Further studies were conducted to determine the efficacy of probes **1** and **2** for the detection of Ce^{3+} ion in biological media. Biological imaging of *Escherichia coli* (*E. coli*) cells was carried out utilizing Laser Confocal Scanning Microscope. To assess this practical application in microbes the cell viability was assessed by MTT assay *in vitro*. Accordingly, three independent triplicates were performed to determine the sensitivity of the probes **1** and **2,** and the medium without the probes as the control. The percentage of cell inhibition was calculated using this formula. % of inhibition = [mean OD of untreated cells (control) / mean OD of treated cells] × 100, and from this the corresponding IC_{50} (concentration that causes a 50% reduction of the cell growth) value was calculated as 43.32 ± 2.35 μM (Fig. S9a) and 41.17 ± 2.15 μM (Fig. S9b). The *E. coli* strain DH5a was cultured in LB media under incubation at 37 °C. Optical microscopy images validate the viability of cells in imaging studies and establish the emission of fluorescence in cultured cells. The cultured cells were exposed to Ce^{3+} ion (20 μM) in 50 mM CH_3CN/ HEPES (1:1 v/v, pH = 7.4) solution for a duration of 30 min at 25 °C [41]. The additional Ce^{3+} ion remaining in the cultured media was eliminated utilizing centrifugation. This cleansing was repeated utilizing 10 mL of 50 mM CH_3CN/HEPES (1:1 v/v, pH = 7.4) solution until only trace level of Ce^{3+} ion was detected on the *E. coli* cell surface. The treated *E. coli* cells were examined using confocal laser scanning microscope (The CLSM cell imaging was taken in Carl Zeiss 710 model German made, Zen 2011 software with F Set 458 nm. The excitation-emission wavelength ranges for cell imaging approximately from 410 to 480 nm, here we used the laser at 458 nm). Imaging studies revealed marginal emission of fluorescence among *E. coli* cells exposed to probes **1** and **2**. Furthermore, introduction of Ce^{3+} ion to cultured cells exposed to probes **1** and **2**, revealed high emission of red fluorescence within the cells (Fig. 10n,o and q,r). This effect can be attributed to the *in situ* [**1** + Ce^{3+} and **2** + Ce^{3+}] complexes formed within the cells. This outcome validates the efficacy of probes **1** and **2** for the detection of Ce^{3+} ion in bacterial cells. Therefore, probes **1** and **2** are suitable for precision imaging of live-cell fluorescence imaging agent in the presence of Ce^{3+} ion in *E. coli* cells and open up avenues for Ce^{3+} ion detection in varied biological cellular life forms.

3.9.3. Antimicrobial Activity of probes 1 and 2 with Ce^{3+} ions

The antibacterial activity of probes **1**, **2** and **1**-Ce^{3+}, **2**-Ce^{3+} complexes were tested against microbial pathogens such as *staphylococcus aureus*, Escherichia coli and controls were kanamycin and Chloramphenicol. The pathogens were incubated on the Nutrient Agar plates and antibiotic discs were used as control. Empty sterile discs added with probes **1**, **2** and **1**-Ce^{3+}, **2**-Ce^{3+} complexes (Fig. S10). After 24 h of incubation, the zone of inhibition was formed around the discs. These results showed that **1**-Ce^{3+} complex showed maximum inhibition and good antibacterial activity against Escherichia coli and *staphylococcus aureus* organisms, whereas **2**-Ce^{3+} complex showed maximum inhibition only to *staphylococcus aureus* (Table 3). The antifungal activity of the probes **1**, **2,** **1**-Ce^{3+} and **2**-Ce^{3+} complexes were tested against *Aspergillus flavus* (Fig. S10). As a result, **1**-Ce^{3+} and **2**-Ce^{3+} complexes showed maximum inhibition and good antifungal activity against *Aspergillus flavus* organisms (Table 3).

4. Conclusion

In conclusion, probes **1** and **2** exhibit high sensitivity to the detection of Ce^{3+} ion as compared to other relevant metal ions monitored by fluorescence studies. The affinity of probes **1** and **2** towards Ce^{3+} ion can be attributed to π to π* transitions leads to strong ICT process assisted by hindrance of n to π* transitions. The binding proposition of the **1**-Ce^{3+} and **2**-Ce^{3+} complexes have been found to be 1:2 based on the job's plot, non-linear least square fitting methods, and MS analysis. The detection limit of probes **1** and **2** towards Ce^{3+} are 1.60×10^{-9} M and 0.17×10^{-9} M, respectively. Probes **1** and **2** were further utilized to detect cerium ions in live-cell imaging. In that, **1**-Ce^{3+} and **2**-Ce^{3+} complexes showed maximum inhibition, good antifungal and antibacterial activity. Moreover, the quinoline-based probes **1** and **2** pave a new pathway to be explored for the detection of various other biological and environmental hazardous substances. Further works on its derivatives and sensing of other potential molecules such as anions, amino acids are currently underway in our laboratory.

Acknowledgements

This work is supported by the SERB-EMR grant by the DST (Sanction No. *SERB-EMR/2016/005692*). Panjab University-SAIF supported the spectral details for this work.

Appendix A. Supplementary data

Supplementary material related to this article can be found, in the online version, at doi:https://doi.org/10.1016/j.jphotochem.2019.112103.

References

[1] S.A. Abbasi, Environmental analysis of cerium using N-p-chlorophenyl-2- furylacrylohydroxamic acid with or without 1-(2-pyridylazo)-2-naphthol, Int. J. Environ. Anal. Chem. 34 (1998) 181–190.
[2] C.L. Wilson, D.W. Wilson, Comprehensive Analytical Chemistry 1 Elsevier, Amsterdam, 1962, p. 477.
[3] V.K. Gupta, A.K. Singh, B. Gupta, A cerium(III) selective polyvinyl chloride membrane sensor based on a Schiff base complex of N,N_-bis[2-(salicylideneamino) ethyl]ethane-1,2-diamine, Anal. Chim. Acta 575 (2006) 198–204.
[4] A. Afkhami, T. Madrakian, A. Shirzadmehr, M. Tabatabaee, H. Bagheri, New Schiff base-carbon nanotube–nanosilica–ionic liquid as a high performance sensing material of a potentiometric sensor for nanomolar determination of cerium(III) ions, Sens. Actuator B-Chem. 174 (2012) 237–244.
[5] A.S. Amin, M.M. Moustafa, R.M. Issa, A rapid, selective and sensitive spectrophotometric method for the determination of Ce(III) using some bisazophenyl-β-diketone derivatives, Talanta 44 (1997) 311–317.
[6] A.N. Masi, R.A. Olsina, Preconcentration and determination of Ce, La and Pr by X-ray fluorescence analysis, using Amberlite XAD resins loaded with 8-quinolinol and 2-(2-(5-chloropyridylazo)-5-dimethylamino)-phenol, Talanta 40 (1993) 931–934.
[7] M. Achilli, G. Ciceri, R. Ferraroli, D. Heltai, W. Martinotti, Determination of cerium, yttrium and thorium in environmental samples, Analyst 114 (1989) 319–323.
[8] K. Dashtian, R.Z. Dorabei, Synthesis and characterization of functionalized mesoprous SBA-15 decorated with Fe_3O_4 nanoparticles for removal of Ce(III) ions from aqueous solution: ICP–OES detection and central composite design optimization, J. Colloid Interface Sci. 494 (2017) 114–123.
[9] M. Ayranov, J. Cobos, K. Popa, V.V. Rondinella, Determination of REE, U, Th, Ba, and Zr in simulated hydrogeological leachates by ICP-AES after matrix solvent extraction, J. Rare Earths 27 (2009) 123–127.
[10] H. Karami, M.F. Mousavi, M. Shamsipur, I. Yavari, A.A. Alizadeh, A new ion-selective electrode for potentiometric determination of Ce(III), Anal. Lett. 36 (2003) 1065–1078.
[11] M.K. Sahani, S. Bhardwaj, A.K. Singh, Novel potentiometric sensor for selective monitoring of Ce^{3+} ion in environmental samples, J. Electroanal. Chem. 780 (2016) 209–216.
[12] H. Bagheri, A. Afkhami, M.S. Tehrani, A. Shirzadmehr, S.W. Husain, H. Khoshsafar, M. Tabatabaee, Novel sensor fabrication for the determination of nanomolar concentrations of Ce^{3+} in aqueous solutions, Anal. Methods 4 (2012) 1753–1758.
[13] T.A. Ali, G.G. Mohamed, E.M.S. Azzam, A.A. Abd-elaal, Thiol surfactant assembled on gold nanoparticles ion exchanger for screen-printed electrode fabrication. Potentiometric determination of Ce(III) in environmental polluted samples, Sens. Actuator B-Chem. 191 (2014) 192–203.
[14] G. Rounaghi, R.M.Z. Kakhki, H. Sadeghian, A new cerium (III) ion selective electrode based on 2,9-dihydroxy-1,10-diphenoxy-4,7-dithia decane, a novel synthetic ligand, Electrochim. Acta 56 (2011) 9756–9761.
[15] A. Akseli, Y. Rakicioglu, Fluorimetric trace determination of cerium (III) with sodium triphosphate, Talanta 43 (1996) 1983–1988.
[16] J.X. Meng, H.J. Wu, D.X. Feng, Fluorimetry determination of trace Ce^{3+} with EDTP, Spectrochim. Acta A. 56 (2000) 1925–1928.
[17] T. Zhang, J. Lu, J. Ma, Z. Qiang, Fluorescence spectroscopic characterization of DOM fractions isolated from a filtered river water after ozonation and catalytic ozonation, Chemosphere 71 (2008) 911–921.
[18] M. Shamsipur, M. Yousefi, M. Hosseini, M.R. Ganjali, Pvc-based 1,3,5-Trithiane coated graphite electrode for determination of cerium (III) ions, Anal. Lett. 34 (2001) 2249–2261.
[19] A.A.A. Gaber, A novel PVC membrane sensor for selective determination of cerium (III) ions, Anal. Lett. 36 (2003) 2585–2596.
[20] M. Akhond, M.B. Najafi, J. Tashkhourian, A new cerium (III)-selective membrane electrode based on 2-aminobenzothiazole, Sens. Actuator B-Chem. 99 (2004) 410–415.
[21] M. Shamsipur, M. Yousefi, M.R. Ganjali, PVC-based 1,3,5-Trithiane sensor for cerium(III) ions, Anal. Chem. 72 (2000) 2391–2394.
[22] M.B. Saleh, A.A.A. Gaber, M.M.R. Khalaf, A.M. Tawfeek, A new ion-selective electrode for potentiometric determination of Ce(III) ions, Sens. Actuator B-Chem. 119 (2006) 275–281.
[23] F. Salehnia, F. Faridbod, A.S. Dezfuli, M.R. Ganjali, P. Norouzi, Cerium(III) ion sensing based on graphene quantum dots fluorescent turn-off, J. Fluoresc. 27 (2017) 331–338.
[24] M.K. Rofouei, N. Tajarrod, M.M. Farahani, R. Zadmard, A new fluorescence sensor for cerium(III) ion using glycine dithiocarbamate capped manganese doped ZnS quantum dots, J. Fluoresc. 25 (2015) 1855–1866.
[25] Y. Huang, X. Wu, T. Tian, Z. Zhu, H. Lin, C. Yang, Target-responsive DNAzyme hydrogel for portable colorimetric detection of lanthanide(III) ions, Sci. China Chem. 60 (2017) 293–298.
[26] J. Wang, P.A.M. Farias, J.S. Mahmoud, Trace determination of lanthanum, cerium, and praseodymium based on adsorptive stripping voltammetry, Anal. Chim. Acta 171 (1985) 215–223.
[27] T. Alizadeh, M.R. Ganjali, M. Akhoundian, P. Norouzi, Voltammetric determination of ultratrace levels of cerium(III) using a carbon paste electrode modified with nano-sized cerium-imprinted polymer and multiwalled carbon nanotubes, Microchim. Acta 183 (2016) 1123–1130.
[28] K. Velmurugan, A. Thamilselvan, R. Antony, V. Rajesh Kannan, L. Tang, R. Nandhakumar, Imidazoloquinoline bearing thiol probe as fluorescent electrochemical sensing of Ag and relay recognition of Proline, J. Photochem. Photobiol. A: Chem. 333 (2017) 130–141.
[29] S. Santhoshkumar, K. Velmurugan, J. Prabhu, G. Radhakrishnan, R. Nandhakumar, A naphthalene derived Schiff base as a selective fluorescent probefor Fe^{2+}, Inorg. Chim. Acta Rev. 439 (2016) 1–7.
[30] K. Velmurugan, R. Nandhakumar, Binol based "turn on" fluorescent chemosensor for mercury ion, J. Lumin. 162 (2015) 8–13.
[31] J. Prabhu, K. Velmurugan, R. Nandhakumar, Pb^{2+} ion induced self assembly of anthracene based chalcone with a fluorescence turn on process in aqueous media, J. Anal. Chem. 70 (2015) 943–948.
[32] J. Prabhu, K. Velmurugan, A. Raman, N. Duraipandy, M.S. Kiran, S. Easwaramoorthi, R. Nandhakumar, A simple chalcone based ratiometric chemosensor for sensitive and selective detection of Nickel ion and its imaging in live cells, Sens. Actuator B-Chem. 238 (2017) 306–317.
[33] K. Velmurugan, S. Suresh, S. Santhoshkumar, M. Saranya, R. Nandhakumar, A simple Chalcone-based ratiometric chemosensor for silver ion, Luminescence 31 (2016) 722–727.
[34] K. Velmurugan, A. Raman, D. Don, L. Tang, S. Easwaramoorthi, R. Nandhakumar, Quinoline benzimidazole-conjugate for the highly selective detection of Zn(II) by dual colorimetric and fluorescent turn-on responses, RSC Adv. 5 (2015) 44463–44469.
[35] K. Velmurugan, S. Mathankumar, S. Santoshkumar, S. Amudha, R. Nandhakumar, Specific fluorescent sensing of aluminium using naphthalene benzimidazole derivative in aqueous media, Spectrochim. Acta A. 139 (2015) 119–123.
[36] N. Bhuvanesh, S. Suresh, J. Prabhu, K. Kannan, V. Rajesh Kannan, R. Nandhakumar, Ratiometric fluorescent chemosensor for silver ion and its bacterial cell imaging, Opt. Mater. 82 (2018) 123–129.
[37] B.D. Nicot, J. Maynadie, D. Lavabre, C. Lepetit, B. Donnadieu, The first X-ray characterized monosubstituted ferrocenyl azacrown chalcone: focus on its calcium Interaction/Electrochemical detection studies, Eur. J. Inorg. Chem. (2005) 2493–2505.
[38] J. Maynadie, B.D. Nicot, D. Lavabre, S.F. Forgues, Monosubstituted ferrocenyl chalcones: effect of structural changes upon the ability to detect calcium by absorption spectroscopy, J. Organomet. Chem. 691 (2006) 1101–1109.
[39] B.D. Nicot, J. Maynadie, D. Lavabre, S.F. Forgues, Ferrocenyl compound as a multiresponsive calcium chemosensor with remarkable fluorescence properties in CH_3CN, Inorg. Chem. 45 (2006) 5691–5702.
[40] P.D. Beer, C. Blackburn, J.F. McAleer, H. Sikaniaka, Redox-responsive crown ethers containing a conjugated link between the ferrocene moiety and a benzo crown ether, Inorg. Chem. 29 (1990) 378–381.
[41] N. Bhuvanesh, S. Suresh, P. Ram Kumar, E.M. Mothi, K. Kannan, V. Rajesh Kannan, R. Nandhakumar, Small molecule "turn on" fluorescent probe for silver ion and application to bioimaging, J. Photochem. Photobiol. A: Chem. 360 (2018) 6–12.